Article

Central role of *d*-band energy level in Cu-based intermetallic alloys

Check for updates

Jing Zhao [1,2], Wenming Xia[1,2], Zhi Zeng [1,2] & Xianlong Wang [1,2] ✉

Cu-Au intermetallic alloys are classic paradigms in the history of alloy theory for studying order-disorder transition, phase stability, and so on. However, density functional theory with a generalized gradient approximation (GGA) fails to describe their formation energies and Au-rich ground states, e.g., calculated formation energies are nearly 40% smaller than experimental values. In this work, we found that these discrepancies, which are also common in other Cu-transition metal (TM) intermetallic alloys, are actually caused by the fact that GGA produces Cu-3*d* bands with a shallower energy level than the experimental results, leading to incorrect *d-d* hybridizations. By using the Hubbard *U* correction to adjust the *d*-bands to the correct position, the discrepancies in GGA calculations are eliminated. Our finding that the correct *d*-bands position is the key to characterize Cu-TMs, which can be achieved efficiently by applying the Hubbard *U* correction.

Cu-based transition metal (Cu-TM) intermetallic alloys are the essential systems employed in a wide range of fields[1–5] such as catalysis[1], electronic components[2], high-temperature structural materials[3], basic metallurgy[4] and magnetoresistance[5]. Among them, Cu-Au intermetallic alloys, an important research topic during the historical development of alloy theory, have always been considered as a classic paradigm for studying crystal structure[6–8], electronic structure[9–12], order-disorder transition[13–17], and for applying different theoretical techniques of phase diagram and phase stability calculations[10,18–22] of intermetallic alloy systems. Most notably, this system can serve as the basic test case for new alloy theory approaches, including the cluster expansion method[23–25], the coupling of configurational and vibrational thermodynamics[22,26], and the phase diagrams calculation methods[20]. Extensive efforts have been made to clarify the structures of Cu-Au intermetallic alloys[8,27–30] because it contains rich experimental information, i.e., complex phase diagrams[28–32] and thermomechanical properties like formation energy (enthalpy of formation)[31], bulk modulus[33], density[10,34], thermal expansion[33,35] and melting temperature[30]. Out of several structures, the fully ordered Cu_3Au and $CuAu_3$ crystallized in the $L1_2$ structure, and the ordered CuAu stabilized in the $L1_0$ phase[8,27] are the most stable structures at low temperature.

However, up to now, despite extensive research on Cu-Au intermetallic alloys, the density functional theory (DFT) calculations have a long time puzzling question in describing the properties of this system: Why is it that the widely used DFT based on the generalized gradient approximation (GGA) or local density functional (LDA) cannot correctly simulate the features of Cu-Au intermetallic alloys?[10,11,22,36] For instance, CuAu formation energy or heat of formation, the difference between the total binding energy

of the system and its pure constituents, calculated by DFT-GGA[22,37] is about 40% smaller than the measured value[31]. Accurately predicting formation energy is crucial in Cu-Au alloys as it determines the stability of alloys with different compositions at different temperatures and pressures[30,31]. Additionally, cluster expansion (CE) simulation combined with LDA predicts a stable Au-rich phase $CuAu_2$ crystallized in β_2 structure, which cannot be observed in experiments, while experimentally proved $CuAu_3$-$L1_2$ structure is predicted to be unstable[22]. Similar to the LDA, previous work clearly established that GGA of PBE also predict the $CuAu_3$ as the unstable phase[37]. These discrepancies hinder the application of DFT calculations in Cu-Au intermetallic alloys. Therefore, there is an urgent need to find out the reason for the DFT failure, not only to understand the Cu-Au intermetallic alloys more sufficiently but also to develop a high-efficient way to simulate their properties, which can significantly promote the investigations of Cu-Au intermetallic alloys and other related metallic alloys. Based on the expensive Heyd-Scuseria-Ernzerhof functional (HSE06) calculations, the significant discrepancies in formation energies and incorrect geometries in the Cu-Au system were ascribed to the failure of GGA to account for nonlocal exact exchange[37].

To obtain an accurate formation energy, a DFT calculation should provide reliable electronic properties of an alloy and its constituent elements simultaneously. In this work, we find that these discrepancies, such as inaccurate formation energy and incorrectly ordered ground states, are due to the GGA calculations producing a shallower Cu-3*d* band energy level than the experimental result, resulting in a weaker *d-d* hybridization between Cu-3*d* and Au-5*d*. Here we employ a Hubbard *U* correction to tune the *d*-band energy level. Taking the CuAu as an example, the GGA with

[1]Key Laboratory of Materials Physics, Institute of Solid State Physics, HFIPS, Chinese Academy of Sciences, Hefei 230031, China. [2]Science Island Branch of Graduate School, University of Science and Technology of China, Hefei 230026, China. ✉e-mail: xlwang@theory.issp.ac.cn

1

Hubbard U correction (GGA + U) formation energy (−93.4 meV/atom) is significantly more negative than those using GGA, and is in excellent agreement with the experimentally measured values (−93.0 meV/atom). Interestingly, this scenario is also widespread in other Cu-TM intermetallic alloys.

Results and discussion
Formation energy

The Cu-TM intermetallic alloys mixed in a 1:1 ratio are easy to synthesize and several phases have been synthesised experimentally: CuY[38], CuSc[39], CuTi[40,41], CuZr[41,42], CuAu[8], CuZn[43], and CuPd[44]. Therefore, in the beginning we have investigated the formation energies of CuTM intermetallic alloys based on the DFT-GGA method, and the relative formation energies of CuTM are shown in Fig. 1a by considering experimental values as a reference, where one can observe that the formation energies of CuY, CuSc, CuTi, and CuZr are larger than the values of experiment[41,42,45–47] (The red bars in Fig. 1a and the formation energies are shown in Supplementary Table 1). For example, the calculated formation energy of CuZr is approximately larger than half of the experimental value. In contrast, for CuAu, CuZn, and CuPd, formation energies simulated by the DFT-GGA are smaller than the experimental values[30,31,48] (the red bars with a asterisk on top in Fig. 1a).

Accordingly, it is natural to separate these intermetallic alloys into two groups: The first group is the system consisting of Cu and TM with d-electron numbers less than or equal to 2 (namely with a shallower d-band energy level), whose formation energies are overestimated; The second group composed of the Cu and TM with d-electron numbers greater than or equal to 9 (that is, with a deeper d-band energy level), where the formation energies are underestimated. These findings show that the failure of DFT-GGA to describe the alloy formation energies is widespread among Cu-TM intermetallic alloys, and the discrepancies between theoretical predictions and experimental measurements are

sensitive to the d-band energy level. Therefore, it is essential to investigate the d-band features in detail.

By observing the electronic density of states of d-band of TMs (Fig. 2), we find that the GGA calculated d-band ranges (the yellow areas) of Cu (~(−1.5) – (−5) eV), Zn (~(−6.7) – (−8.5) eV), Ag (~(−2.8) – (−6.2) eV) and Cd (~(−8.2) – (−9.9) eV) are outside the experimental measurements (denoted by a horizontal solid line in Fig. 2)[49–53] [Cu ((−2) – (−6) eV), Zn ((−8.5) – (−11.5) eV), Ag ((−3.9) – (−7.4) eV), and Cd ((−9.0) – (−13.0) eV]. The main peak of the density of states closest to the Fermi energy level in TM (TM=Cu, Zn, Ag and Cd) is not within the range of experimental observations (see Fig. 2a-d). In contrast, for the Sc-3d, Zr-4d, Pd-4d, Au-5d, Y-4d, and Ti-3d bands (Fig. 2e-h and Supplementary Fig. 1), the main peaks and distribution areas of the d-band DOS simulated by GGA are in general agreement with the measurements[49,54–60]. One can easily observe that the GGA fails to characterize the d-band energy levels of TMs, the d-bands of which are fully occupied and far from the Fermi energy level, but describes well the case where there are d-electron contributions at the Fermi energy level. In order to accurately describe the d-band characteristics of TMs, more accurate functionals, e.g., the HSE06 functional[61,62], can be used. However, they are computationally expensive, which limits their applications for structure search, complex alloy simulations, and high throughput calculations. The GGA + U approach, which in addition to having a similar computational power to GGA, shifts the occupied d state to the lower energy region and only slightly affects the other orbitals when U is only applied to d orbitals, can be used to elucidate the physical mechanism. Therefore, we choose GGA + U to modulate the characteristics of the d-band, including the range of the distribution and the position of the peaks. The motivation for applying the U correction to the fully occupied d orbitals of transition metals is to adjust them to the correct energy level. As illustrated in the green areas of Fig. 2a–d, after applying U values of 3.72 eV, 6.00 eV, 3.72 eV, and 5.00 eV to d-orbitals of Cu, Zn, Ag, and Cd, respectively, the calculated d-band energy range are consistent well with experimental measurements[49–53].
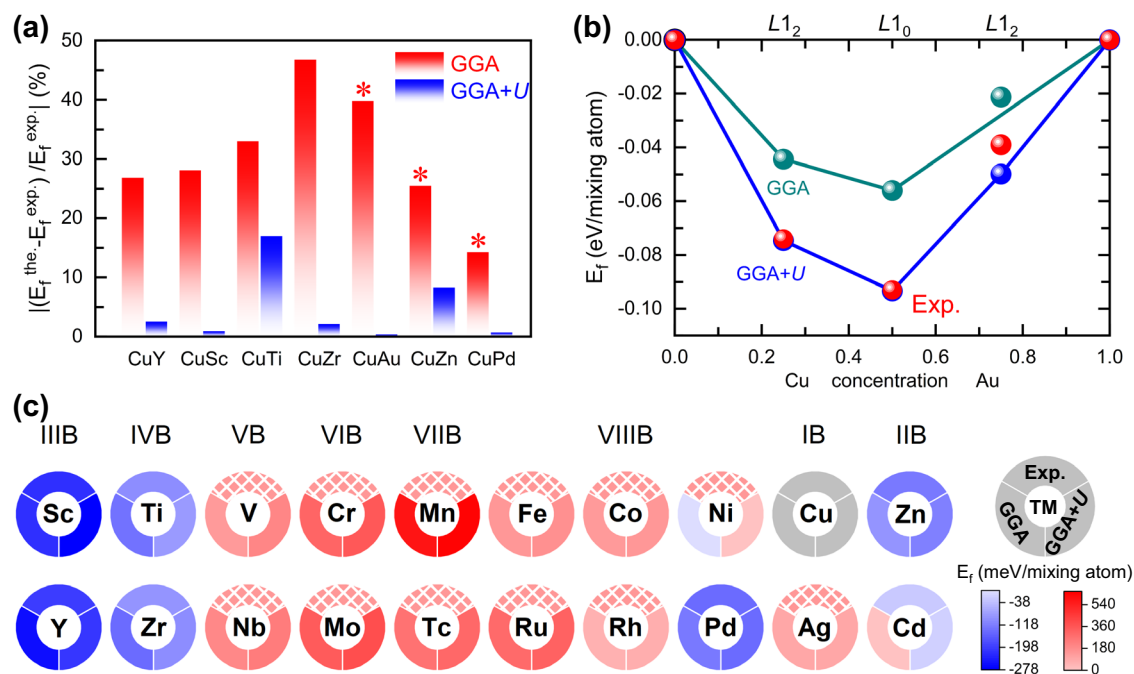

Fig. 1 | Formation energies (E_f) of Cu-based transition metal (Cu-TM) intermetallic alloys. a E_f discrepancies between theoretical predictions and experimental results. The red bars with and without asterisk on top indicate that the GGA overestimates and underestimates the E_f, respectively. b GGA and GGA + U calculated ground state lines of Cu-Au intermetallic alloy together with the experimental results. The filled cyan and blue spheres/lines mean calculated E_f based on the GGA and GGA + U, respectively. Experimentally measured E_f are presented as filled red spheres. c Summary of the E_f values for Cu-TM alloys using GGA (left pie charts) and GGA + U (right pie charts) approaches. We also give the experimentally determined energies of formation of ordered structures, as shown in the top pie charts filled with solid colors. Note that the pie charts above, filled with grids, indicate that the transition metals could not form an ordered alloy with Cu. In (c), except for Cu_8Ni and Cu_2Cd, the rest of Cu-TM are mixed in a ratio of 1:1.
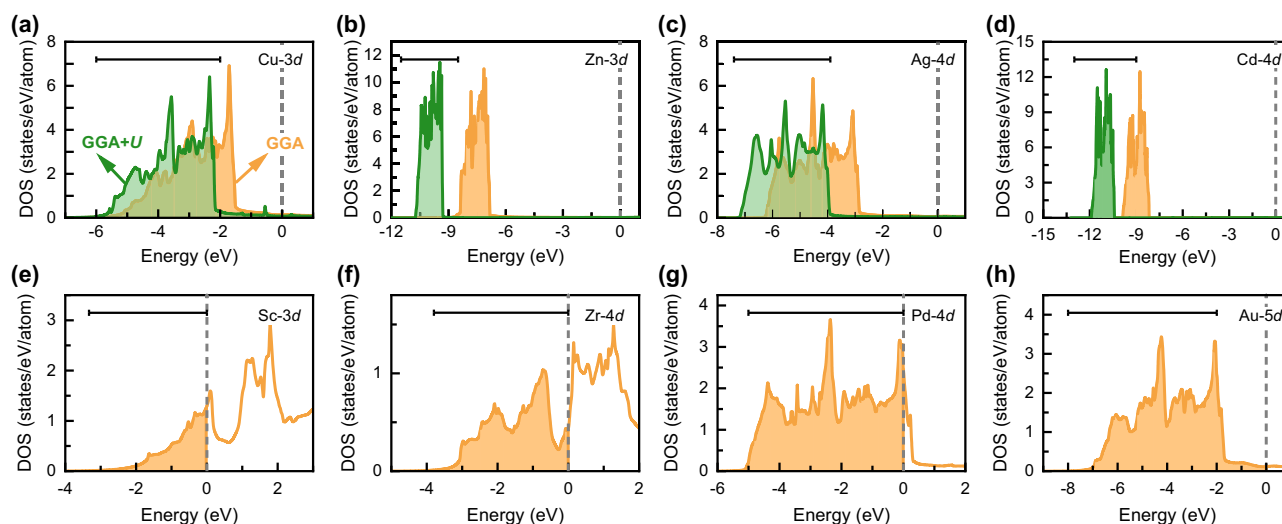
Fig. 2 | Densities of states (DOS) of transition metals. DOS of *d*-bands [from left to right, top to bottom: Cu-3*d*, Zn-3*d*, Ag-4*d*, Cd-4*d*, Sc-3*d*, Zr-4*d*, Pd-4*d* and Au-5*d*] calculated using GGA (yellow ranges) and GGA + *U* (green ranges), as shown in (**a**–**h**). The onsite Coulomb Interaction *U* of 3.72 eV, 6.00 eV, 3.72 eV, and 5.00 eV are used for the Cu-3*d*, Zn-3*d*, Ag-4*d*, and Cd-4*d* electrons, respectively. The horizontal black solid lines indicate the experimentally reported *d*-band ranges based on the X-ray photoemission spectra or ultraviolet photoemission spectra, and the vertical dashed line is the Fermi level.

In the absence of experimental results, the *U* values may can be obtained by the linear response constrained density functional theory (cDFT) method, which has been demonstrated to be computationally efficient and accurate for the calculation of the *U* parameter with high applicability[63–69]. On the other hand, the expensive HSE06 calculated density of states can also be used as a reference for the determination of effective *U* values.

After applying the Hubbard *U* corrections to Cu, Zn, Ag, and Cd, we can predict the formation energies of Cu-TM intermetallic compounds consistent with the experiment. In Cu-Au system based on GGA and GGA + *U*, the calculations give ground-state convex hull curves (Fig. 1b), which are constructed by the formation energies of thermodynamically stable structures, where the intermetallic alloys located on the hulls are stable against decomposition. We can find that the calculated formation energies of Cu-Au based on GGA (the cyan spheres/lines in Fig. 1b) are significantly smaller than experimental values, and experimentally synthesized CuAu$_3$ does not locate on the convex hull. However, GGA + *U* calculations can not only give out the correct formation energies but also reproduce the CuAu$_3$ reported by experiment[31] (the blue lines/spheres in Fig. 1b). The good agreement between GGA + *U* calculations and experimental measurements in Cu-Au implies that the correct *d*-band position may play an important role in formation energy. It should be noted that the GGA + *U* formation energy of the fully ordered CuAu$_3$ crystallised in the $L1_2$ structure is −50 meV/atom, which is slightly lower than the experimentally measured −39 meV/atom. The experimental formation energy of CuAu$_3$ comes from an incompletely ordered experimental structure[31], which may be responsible for its location above the convex hull as shown in Fig. 1b. Since Cu-3*d* energy level based on the GGA is shallower than experimental observation, the *d*-band center distance between the Cu-3*d* and Au-5*d* is overestimated (Fig. 3a, Supplementary Fig. 2a, b and Supplementary Table 2), resulting in a weaker 3*d*-5*d* hybridization and smaller formation energies than experimental values (the cyan and red spheres in Fig. 1b).

By applying *U* = 3.72 eV, the Cu-3*d* band is moved to the lower energy region. At the same time, the distribution features of Au-*s*, Au-*p*, Cu-*s*, and Cu-*p* orbitals in the intermetallic alloy are slightly affected (see Supplementary Fig. 3). Therefore, the Hubbard *U* correction, which plays a role in modulating the position of the *d*-energy level, is applied to Cu element with fully filled *d*-shell. After applying the *U* value to the Cu-*d* orbital, the position of the Cu-*d* band energy level (see Supplementary Table 2) shifted from −2.48 eV to −3.13 eV, closer to the Au-*d* band energy level (−4.33 eV). As shown in Fig. 3a, we can also observe a weakening of the intensity of the *d*-

band DOS in the CuAu alloy after the addition of *U*. Furthermore, the Hubbard *U* correction causes 0.6% volume collapse and 0.004 Å Cu-Au bond length shrinking in CuAu. These results demonstrate that the hybridization between Cu-3*d* and Au-5*d* orbitals became stronger. The same phenomena can also be observed in Cu$_3$Au and CuAu$_3$ intermetallic alloys (Supplementary Fig. 2a, b). Our results have demonstrated that the inaccurate description of the Cu-3*d* band energy level using GGA is a severe problem for the accurate description of the Cu-Au formation energies. Furthermore, a similar scenario occurs in CuPd intermetallic compounds where the *d*-band center of Pd-4*d* is lower than the Cu-3*d* band center (the red bars with a asterisk on top in Fig. 1a, Supplementary Fig. 2c and Supplementary Table 2).

To provide further validation of our findings, we have investigated the effect of Cu-3*d* distribution on the accuracy of the formation energies of other CuTM (TM = Sc, Ti, Y and Zr) intermetallic compounds, where the *d*-band center of TM-*d* is higher than the Cu-3*d* band energy center (Fig. 3b, Supplementary Fig. 2d–f and Supplementary Table 2). The shallower Cu-3*d* energy-level based on the GGA enhances the interactions between Cu-3*d* and TM-*d*, leading to larger formation energies than the experimental values (the red bars in Fig. 1a). The modulation of Cu-3*d* orbital by the Hubbard *U* correction reduces the hybridization between Cu-3*d* and TM-*d* (TM = Sc, Ti, Y and Zr), resulting in the relative discrepancies between theoretically simulated formation energies and experimental values to be reduced from 26.8% to 2.6% (CuY), 28.1% to 0.9% (CuSc), 33.0% to 17.0% (CuTi), and 46.8% to 2.1% (CuZr) (the blue bars in Fig. 1a and Supplementary Table 1).

Considering CuSc, we have further performed the crystal orbital Hamilton population (COHP)[70,71] analyses to study the bond strength. The interactions between Cu-3*d* and Sc-3*d* in CuSc and their corresponding energy values after integration up to the Fermi level (ICOHP, an efficient measure of the bond strength) are shown in Fig. 3d. Compared with the *d*-bonding contribution of CuSc based on the GGA (ICOHP = −0.147 eV), the bonding strength (ICOHP = −0.130 eV) of the GGA + *U* calculation become weaker, which rationalizes our conclusion that correct Cu-3*d* energy-level is the key for describing the CuTM formation energies correctly. Furthermore, after applying Hubbard *U* corrections on Cu-3*d* and Zn-3*d*, a more accurate CuZn formation energy is obtained, as shown in Figs. 1a, 3c.

Based on the experimental phase diagram[30,72,73], except for the CuTM intermetallic alloys, Cd can also form ordered compounds with Cu but not with the ratio of 1:1 as shown in Fig. 1a. We have also calculated the

Fig. 3 | DOS of CuTM intermetallic compounds and COHP analysis. a–c DOS calculated using GGA (up panel) and GGA + U (down panel) of CuAu-$L1_0$, CuSc-$B2$, and CuZn-$B2$. In (**a–c**), the dashed vertical lines show the Fermi energy level. **d** The Crystal Orbital Hamilton Population (COHP) analysis of d-bonding interactions in CuSc based on the GGA and GGA + U calculations and their energy values after integration up to the Fermi level (ICOHP).
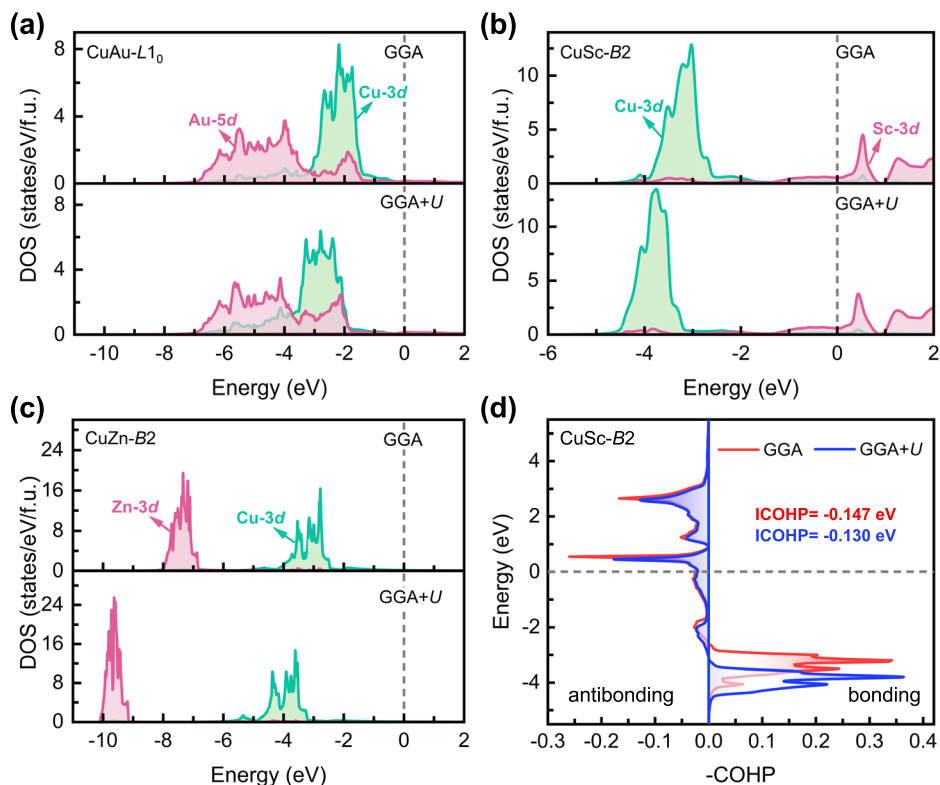
formation energy of the experimentally reported Cu_2Cd[30,37,74] compound closer to a 1:1 ratio, and the results are shown in Fig. 1c and Supplementary Table 1. In contrary to experimental observation[30,37], the GGA describes the Cu_2Cd intermetallic alloy as a phase separation system with a positive energy of formation of 0.008 eV/atom. By adjusting the Cu-3d and Cd-4d bands to correct energy levels, GGA + U calculations give a negative formation energy of −0.012 eV/atom, which is close to the experimental value (−0.026 eV/atom). On the other hand, there are several 3d and 4d TMs (TM = V-Ni, Nb-Rh, and Ag) that cannot form ordered alloys with Cu, where phase separation tendencies are experimentally observed in the Cu-TMs phase diagram[72,75,76]. Formation energies of these alloys using different DFT approaches (GGA and GGA + U) are given in Supplementary Table 1. Except for the Cu-Ni case, based on CuTM (TM = V-Co, Nb-Rn, and Ag) structures shown in the Open Quantum Materials Database (OQMD)[41,42], calculated formation energies by using both GGA and GGA + U (Pie chart filled by gradient red in Fig. 1c) are positive consistent with experimental reports. In case of Cu-Ni, only Cu_8Ni can be found in the OQMD[41,42] with a formation energy of −0.6 meV/atom, which is also consistent to some extent with our calculated formation energy of Cu_8Ni based on the GGA (−0.5 meV/atom, Pie chart filled by gradient blue). Nevertheless, GGA + U calculations give a positive formation energy of 2.6 meV/atom, agreeing with the experimental observations[72,77]. These results strongly confirm the improvement in accuracy when the d-bands are fitted to the correct position, suggesting that GGA + U is an effective method for predicting the formation energies of Cu-TMs.

Cohesive energy and ground-state structures

Several studies have shown that finding a universal functional which can provide accurate cohesive energies and formation energies of intermetallic alloys is challenging[48,78]. We further test the accuracy of GGA + U in cohesive energies[79,80] of Cu_3Au, CuAu and $CuAu_3$ intermetallic compounds. The results show that the mean absolute percentage error of 15.73% in the GGA + U cohesive energies is larger than the GGA error of 11.43% and is smaller than the HSE06 error of 18.20%, as shown in Supplementary Table 3, indicating that neither DFT + U nor HSE06 is the ultimate solution for

intermetallic alloys with Cu atom if cohesive energies are also analyzed (for details of a discussion, see the Supplemental Material).

Since GGA + U has a similar computational efficiency as that of GGA, modulation of d-bands by the Hubbard U correction can be applied not only to the characterization of formation energies but also to the prediction of the ground-state structures of intermetallic alloys, such as high-efficient structure prediction and high-throughput computing. Therefore, the stable ordered Cu-Au structures are simulated based on the CE[81] method combined with the GGA and GGA + U, as shown in the Fig. 4. Both GGA (Fig. 4a) and GGA + U (Fig. 4b) calculations correctly give the experimentally observed Cu-rich stable phases of Cu_3Au-$L1_2$ and CuAu-$L1_0$[27,31], which are located on the hulls. However, in the Au-rich region, the experimentally reported $CuAu_3$-$L1_2$ phase with Pm-$3m$ symmetry located above the convex hull curve of the GGA simulations, while a $P4/mmm$-type $CuAu_3$ structure was incorrectly predicted as the ground state. Two Au-rich components ($CuAu_2$ and Cu_2Au_3), not observed by experimental observation, are predicted to be stable phases. We know that the vibrational entropy omitted in the static calculation is also a factor influencing the energy to be reckoned with. Therefore, we have considered the energies of Cu, Au and Cu-Au alloys at 300 K and 1000 K to calculate the corresponding formation energies. The results show that with increasing temperature, the stability of both the Pm-$3m$-type and the $P4/mmm$-type $CuAu_3$ decreased, as reflected by being above the convex hull curve at 300 K, and $CuAu_2$ became the only stable structure with increasing temperature up to 1000 K in the Au-rich region. The convex hull curve at high temperatures was inconsistent with experimental observation[8,27,31].

In contrast with GGA results, experimentally reported $CuAu_3$-$L1_2$ phase with Pm-$3m$ symmetry located on the convex hull curve of GGA + U simulations as shown in Fig. 4b, d. The $CuAu_2$ and Cu_2Au_3 tend to decompose at high temperatures, consistent with the fact that these structures have not been observed experimentally. Consequently, the $CuAu_3$-$L1_2$ phase with Pm-$3m$ symmetry is becoming the only stable phase in the Au-rich range at 1000 K, which agree precisely with experimental observations[8,27,31]. These findings have indicated that it is essential to adjust
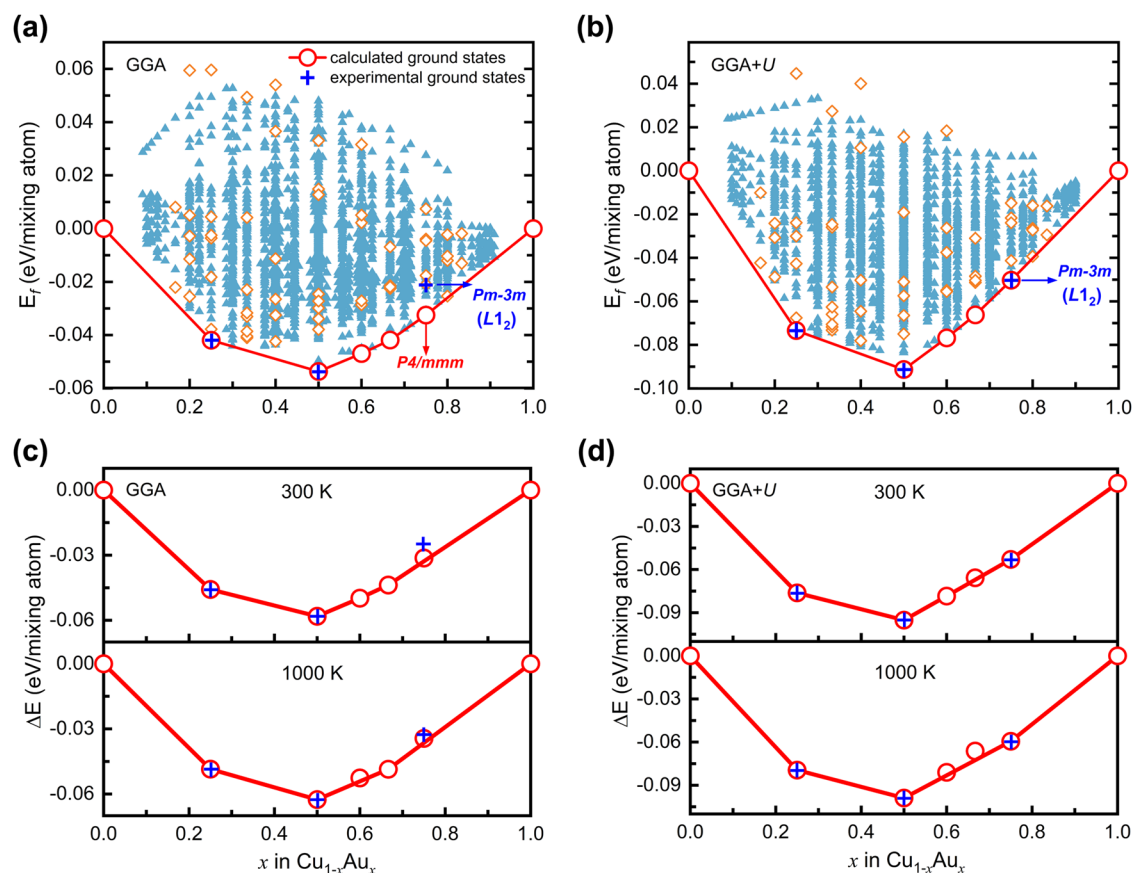
Fig. 4 | Ground state structures of Cu-Au system. Predicted ground state lines of $Cu_{1-x}Au_x$ using (**a**) GGA and (**b**) GGA + U combined with the cluster expansion method. The orange diamond and blue triangles mean the mixing energies calculated by GGA or GGA + U and predicted using the effective cluster interactions, respectively. Convex hull curves of the Cu-Au intermetallic system at temperatures 300 and 1000 K based on GGA and GGA + U are shown in (**c**, **d**), respectively. In (**a**–**d**), the blue crosses represent the structures observed in the experiment and the open red circles represent the ground states predicted by GGA or GGA + U, respectively.

d-bands to the correct energy level for describing the ground state of the Cu-Au system, and Hubbard U correction is a highly efficient way to realize this.

Finally, we analyzed the variation of the electron occupation numbers of Cu and Au based on the Millikan charge, which are summarized in Supplementary Table 4. We can find that the occupation number of elemental Cu or Au d electrons is less than 10, implying d to sp promotion (or hybridization), this hybridization has also been reported in the study of Cu nanoparticles[82]. Relative to the pure element, Cu gains d and Au loses d charge upon alloying, in agreement with the experiment[83] and similar to the charge transfer in AuAg and AgPd[84]. Therefore, intra-atomic charge redistribution during elemental and alloy formation results in d-bands containing partial unoccupied state, which is involved in bonding. In addition, the s and p electrons in the outer shell of Cu and Au are also involved in bonding.

In this work, the formation energies of Cu-TM intermetallic alloys (TM = Sc-Zn, Y-Cd, and Au) are systematically investigated based on the first-principles methods. We have found that d-band energy levels of TMs (Cu, Zn, Ag, and Cd) with fully occupied d-bands cannot be correctly described by the GGA calculations. In contrast, the counterparts of TMs (e.g., Sc, Zr, Pd, and Au) with d-electron distribution at the Fermi energy level can be successfully described. The deficiencies of GGA in the description of Cu-Au intermetallic alloys, which are also prevalent in other Cu-TM intermetallic alloys, are caused by the mischaracterization of the d-band energy-level resulting in wrong d-d hybridization. Applying the Hubbard U to Cu-3d can rectify the GGA deficiency in describing the properties of Cu-TM intermetallic alloys by adjusting the energy level of the d-band to correct position. For example, in the Cu-Au system, the GGA + U formation energy of CuAu is −93.4 meV/atom, which is similar to the experimental result

(−93.0 meV/atom). Furthermore, the CuAu$_3$-$L1_2$ phase with Pm-$3m$ symmetry is correctly predicted as the only stable phase in the Au-rich range. Our results have demonstrated that the interactions between Cu-3d and TM-d play a crucial role in characterization of formation energy and ground state structures of Cu-TM intermetallic alloys. Our results illustrate the high efficiency of the GGA + U in tuning the TM-d band to an accurate energy level and offer an idea for investigating other transition metal intermetallic alloys, phase diagrams and high throughput calculations, etc.

Methods
Density functional theory calculations
The density functional theory calculations were carried out with the projector augmented wave (PAW) scheme[85,86] as implemented in the Vienna Ab initio Simulation Package (VASP)[87]. The exchange and correlation energy was described within the generalized gradient approximation (GGA) of Perdew-Burke-Ernzerhof[88]. GGA with the Hubbard U correction (GGA + U) based on the Dudarev's approach[89], was used to fit the d-bands of transition metals to the correct energy level. Please note that in Kohn-Sham density-functional theory, only the energy of the highest occupied state has a rigorous physical interpretation, i.e., it is equal to the first ionization energy[90–94]. The onsite Coulomb interaction U of 3.72 eV, 6.00 eV, 3.72 eV and 5.00 eV was carried out for the Cu-3d, Zn-3d, Ag-4d and Cd-4d, respectively. To ensure the quality of the selected U values, we have taken CuAu alloy as an example and calculated the formation energies at U values of 3.52 eV, 3.62 eV, 3.82 eV and 3.92 eV, with corresponding results of −0.091 eV/atom, −0.092 eV/atom, −0.094 eV/atom and −0.095 eV/atom, which are in general agreement with the experimental observation (−0.093 eV/atom). Additionally, we also use the local density

approximation[95] (LDA) and LDA with Hubbard U correction ($U = 3.72$ eV) to calculate the formation energy of the CuAu intermetallic compound, and find that the calculated results are in excellent agreement with those obtained using GGA and GGA $+ U$ ($U = 3.72$ eV), respectively. Our findings indicate that the choice of the exchange and correlation functional does not significantly affect the formation energy.

The plane-wave energy cutoff of 400 eV and reciprocal space resolution of $2\pi \times 0.025$ Å^{-1} for all calculations were used. Both lattice parameters and atomic positions were fully relaxed until forces on each atom were less than 0.001 eV/Å, and the convergence value of energy was set to 1.0×10^{-6} eV. All structures were optimized entirely until the total stress tensors were below 0.1 GPa. The crystal orbital Hamilton population (COHP) analysis was performed using the LOBSTER package to evaluate the bonding interactions quantitatively[71]. To predict a stable ordered crystal structure of the Cu-Au system, we have performed the calculations using a cluster expansion method[81] combined with both GGA and GGA $+ U$, as implemented in the Alloy Theoretic Automated Toolkit (ATAT) package and its interface with the MAPS code[25,96].

Data availability
The authors declare that the data supporting the findings of this study are available within the article and its supplementary information file or from the corresponding author on reasonable request.

Code availability
The VASP code is charged. The LOBSTER and ATAT codes are freely available and can be used on the website.

References
1. Goulas, K. A. et al. Synergistic effects in bimetallic palladium-copper catalysts improve selectivity in oxygenate coupling reactions. *J. Am. Chem. Soc.* **138**, 6805–6812 (2016).
2. Volkov, A. Y. Structure and mechanical properties of CuAu and CuAuPd ordered alloys. *Gold. Bull.* **37**, 208–215 (2004).
3. Metadjer, N. et al. Tight-binding calculation of structural properties of bulk Cu$_3$Au and its corresponding clusters. *Superlattice. Microst.* **30**, 21–28 (2001).
4. Semboshi, S. & Takasugi, T. Fabrication of high-strength and high-conductivity Cu-Ti alloy wire by aging in a hydrogen atmosphere. *J. Alloy. Comp.* **580**, S397–S400 (2013).
5. Fan, X. et al. Magnetic properties of Co-Cu metastable solid solution alloys. *Phys. Rev. B* **69**, 094432 (2004).
6. Wright, P. & Goddard, K. F. Lattice parameter and resistivity study of order in the alloy CuAu$_3$. *Acta Metall.* **7**, 757–761 (1959).
7. Kogachi, M. & Nakahigashi, K. Phase relations in the AuCu$_{1-y}$Ag$_y$ and Au(Cu$_{1-y}$Ag$_y$)$_3$ Ternary Systems. *Jpn. J. Appl. Phys.* **24**, 121–125 (1985).
8. Kubiak, R. & Janczak, J. X-ray study of ordered phase formation in Au$_{31.6}$Cu$_{68.4}$, Au$_{50}$Cu$_{50}$ and Au$_{75}$Cu$_{25}$. *J. Alloy. Compd.* **176**, 133–140 (1991).
9. Skriver, H. L. & Lengkeek, H. P. Band structure and optical properties of ordered AuCu$_3$. *Phys. Rev. B* **19**, 900–910 (1979).
10. Wei, S.-H., Mbaye, A. A., Ferreira, A. C. & Zunger, A. First-principles calculations of the phase diagrams of noble metals: Cu-Au, Cu-Ag, and Ag-Au. *Phys. Rev. B* **36**, 4163–4185 (1987).
11. Terakura, K., Oguchi, T., Mohri, T. & Watanabe, K. Electronic theory of the alloy phase stability of Cu-Ag, Cu-Au, and Ag-Au systems. *Phys. Rev. B* **35**, 2169–2173 (1987).
12. Weinberger, P., Drchal, V., Szunyogh, L., Fritscher, J. & Bennett, B. I. Electronic and structural properties of Cu-Au alloys. *Phys. Rev. B* **49**, 13366–13372 (1994).
13. Shockley, W. Theory of order for the copper gold alloy system. *J. Chem. Phys.* **6**, 130–144 (1938).
14. Newkirk, J. B. Order-disorder transformation in Cu-Au alloys near the composition CuAu. *J. Met.* **5**, 823–826 (1953).
15. Vanbaal, C. M. Order-disorder transformations in a generalized Ising alloy. *Physica* **64**, 571–586 (1972).
16. Chakraborty, B. & Xi, Z. Atomistic landau theory of ordering and modulated phases in Cu-Au alloys. *Phys. Rev. Lett.* **68**, 2039–2042 (1992).
17. Polatoglou, H. M. & Bleris, G. L. Constant temperature and pressure monte carlo study of the order-disorder transition of Cu$_3$Au. *Interface Sci.* **2**, 31–44 (1994).
18. Kikuchi, R. Superposition approximation and natural iteration calculation in cluster-variation method. *J. Chem. Phys.* **60**, 1071–1080 (1974).
19. Ackland, G. J. & Vitek, V. Many-body potentials and atomic-scale relaxations in noble-metal alloys. *Phys. Rev. B* **41**, 10324–10333 (1990).
20. Oates, W. A., Spencer, P. J. & Fries, S. G. A cluster expansion for Cu-Au alloys based on experimental data. *Calphad* **20**, 481–489 (1996).
21. Paxton, A. T. & Polatoglou, H. M. Origin of the modulated phase in copper-gold Alloys. *Phys. Rev. Lett.* **78**, 270–273 (1997).
22. Ozoliņš, V., Wolverton, C. & Zunger, A. Cu-Au, Ag-Au, Cu-Ag and Ni-Au intermetallics: First-principles study of phase diagrams and structures. *Phys. Rev. B* **57**, 6427–6443 (1998).
23. Sanchez, J. M. & De Fontaine, D. The fee Ising model in the cluster variation approximation. *Phys. Rev. B* **17**, 2926–2936 (1978).
24. Sigli, C. & Sanchez, J. M. Theoretical description of phase equilibrium in binary alloys. *Acta Metall.* **33**, 1097–1104 (1985).
25. Van de Walle, A. & Ceder, G. Automating first-principles phase diagram calculations. *J. Phase. Equilib.* **23**, 348–359 (2002).
26. Ozoliņš, V., Wolverton, C. & Zunger, A. First-principles theory of vibrational effects on the phase stability of Cu-Au compounds and alloys. *Phys. Rev. B* **58**, R5897–R5900 (1998).
27. Lu, S. S. & Liang, C. K. The superlattice formation and lattice spacing changes in copper-gold alloys. *Acta Phys. Sin. Chin. Ed.* **22**, 669–697 (1966).
28. Batterman, B. W. X-ray study of order in the alloy CuAu$_3$. *J. Appl. Phys.* **28**, 556–561 (1957).
29. Ogawa, S. & Watanabe, D. Electron diffraction study on the ordered alloy Au$_3$Cu. *J. Appl. Phys.* **22**, 1502–1502 (1951).
30. Hultgren, R., Desai, P. D., Hawkins, D. T., Gleiser, M. & Kelley, K. K. Selected values of the thermodynamic properties of binary alloys. (American Society for Metals, Metals Park, OH, 1973).
31. Orr, R. L. Heats of formation of solid Au-Cu alloys. *Acta Metall.* **8**, 489–493 (1960).
32. Kuczynski, G., Doyama, M. & Fine, M. Transformations in disordered gold copper alloys. *J. Appl. Phys.* **27**, 651–655 (1956).
33. Simmons, G. & Wang, H. F. Single crystal elastic constants and calculated aggregate properties: A Handbook 2nd edn. (Cambridge, MA: MIT Press). (1991).
34. Barrera, G. D., De Tendler, R. H. & Isoardi, E. P. Structure and energetics of Cu-Au alloys. *Model. Simul. Mater. Sci. Eng.* **8**, 389–401 (2000).
35. Jin, H. M. & Wu, P. First principles calculation of thermal expansion coefficient: Part 1. Cubic metals. *J. Alloy. Compd.* **343**, 71–76 (2002).
36. Lu, Z. W., Wei, S.-H., Zunger, A., Frota-Pessoa, S. & Ferreira, L. G. First-principles statistical mechanics of structural stability of intermetallic compounds. *Phys. Rev. B* **44**, 512–544 (1991).
37. Zhang, Y. S., Kresse, G. & Wolverton, C. Nonlocal first-principles calculations in Cu-Au and other intermetallic alloys. *Phys. Rev. Lett.* **112**, 075502 (2014).
38. Moriarty, J. L., Humphreys, J. E., Gordon, R. O. & Baenziger, N. C. X-ray examination of some rare-earth-containing binary alloy systems. *Acta Cryst.* **21**, 840–841 (1966).

39. Aldred, A. T. Intermediate phases involving scandium. *Trans. AIME* **224**, 1082 (1962).

40. Eremenko, V. N., Buyanov, Y. I. & Prima, S. B. Phase diagram of the system titanium-copper. *Sov. Powder Metall. Met. Ceram.* **5**, 494–502 (1966).

41. Saal, J. E., Kirklin, S., Aykol, M., Meredig, B. & Wolverton, C. Materials design and discovery with high-throughput density functional theory: the open quantum materials database (OQMD). *Jom* **65**, 1501–1509 (2013).

42. Kirklin, S. et al. The Open Quantum Materials Database (OQMD): assessing the accuracy of DFT formation energies. *npj Comput. Mater.* **1**, 1–15 (2015).

43. Shimizu, S., Murakami, Y. & Kachi, S. Lattice softening and martensitic transformation in Cu-Ni-Zn β phase alloys. *J. Phys. Soc. Jpn.* **41**, 79–84 (1976).

44. Yamauchi, M. & Tsukuda, T. Production of an ordered (B2) CuPd nanoalloy by low-temperature annealing under hydrogen atmosphere. *Dalton Trans.* **40**, 4842–4845 (2011).

45. Watanabe, S. & Kleppa, O. J. Thermochemistry of alloys of transition metals: Part IV. Alloys of copper with scandium, yttrium, lanthanum, and lutetium. *Metall. Trans. B* **15B**, 357–368 (1984).

46. Guo, Q. & Kleppa, O. J. The standard enthalpies of formation of the compounds of early transition metals with late transition metals and with noble metals as determined by Kleppa and co-workers at the University of Chicago-A review. *J. Alloy. Compd.* **321**, 169–182 (2001).

47. Kleppa, O. J. & Watanabe, S. Thermochemistry of alloys of transition metals: Part III. Copper-Silver,-Titanium, -Zirconium, and-Hafnium at 1373 K. *Metall. Trans. B* **13**, 391–401 (1982).

48. Nepal, N. K., Adhikari, S., Neupane, B. & Ruzsinszky, A. Formation energy puzzle in intermetallic alloys: Random phase approximation fails to predict accurate formation energies. *Phys. Rev. B* **102**, 205121 (2020).

49. Eastman, D. E. & Cashion, J. K. Photoemission from Cu, Ag, and Au in the 10- to 27-eV energy range. *Phys. Rev. Lett.* **24**, 310–313 (1970).

50. Andrews, P. T. & Hisscott, L. A. X-ray photoelectron spectroscopy of some Cu-Zn alloys. *J. Phys. F: Met. Phys.* **5**, 1568–1572 (1975).

51. Leiro, J. A., Kokko, K. & Laihia, R. Electronic structures of AuMg and AuZn. *J. Electron Spectrosc.* **113**, 167–174 (2001).

52. Riley, J. D., Leckey, R. C. G., Jenkin, J. G., Liesegang, J. & Poole, R. T. Ultraviolet photoelectron spectra of the outer d bands of Ag-In and Ag-Cd alloys. *J. Phys. F: Met. Phys.* **6**, 293–301 (1976).

53. Crecelius, G. & Wertheim, G. K. Effects of atomic order in α-and β-phase Ag-Cd alloys studied by x-ray photoelectron spectroscopy. *Phys. Rev. B* **18**, 6525–6530 (1978).

54. Das, S. G. Electronic structure and magnetic properties of scandium. *Phys. Rev. B* **13**, 3978–3983 (1976).

55. Oelhafen, P., Hauser, E., Güntherodt, H.-J. & Bennemann, K. H. New type of *d*-band-metal alloys: the valence-band structure of the metallic glasses Pd-Zr and Cu-Zr. *Phys. Rev. Lett.* **43**, 1134–1137 (1979).

56. Weightman, P. & Andrews, P. T. The Pd Auger spectra of $Mg_{75}Pd_{25}$, $Al_{80}Pd_{20}$ and Pd and their dependence on band structure. *J. Phys. C: Solid St. Phys.* **13**, L815–L819 (1980).

57. Steiner, P., Höchst, H., Schneider, J., Hüfner, S. & Politis, C. The XPS valence band spectra of Hf metal and $HfC_xN_yO_z$ compounds and the correlation to their superconductivity. *Z. Phys. B Condens. Matter* **33**, 241–250 (1979).

58. Höchst, H., Hüfner, S. & Goldmann, A. XPS-valence bands of iron, cobalt, palladium and platinum. *Phys. Lett. A* **57A**, 265–266 (1976).

59. Fujimori, A. & Schlapbach, L. Electronic structure of yttrium hydride studied by X-ray photoemission spectroscopy. *J. Phys. C: Solid State Phys.* **17**, 341–351 (1984).

60. Eastman, D. E. Photoemission studies of *d*-band structure in Sc, Y, Gd, Ti, Zr, Hf, V, Nb, Cr and Mo. *Solid State Commun.* **7**, 1697–1700 (1969).

61. Heyd, J., Scuseria, G. E. & Ernzerhof, M. Assessment and validation of a screened Coulomb hybrid density functional. *J. Chem. Phys.* **118**, 8207–8215 (2003).

62. Paier, J. et al. Screened hybrid density functionals applied to solids. *J. Chem. Phys.* **124**, 154709 (2006).

63. Cococcioni, M. & De Gironcoli, S. Linear response approach to the calculation of the effective interaction parameters in the LDA+*U* method. *Phys. Rev. B* **71**, 035105 (2005).

64. Nakamura, K., Arita, R., Yoshimoto, Y. & Tsuneyuki, S. First-principles calculation of effective onsite Coulomb interactions of 3*d* transition metals: Constrained local density functional approach with maximally localized Wannier functions. *Phys. Rev. B* **74**, 235113 (2006).

65. Kulik, H. J., Cococcioni, M., Scherlis, D. A. & Marzari, N. Density functional theory in transition-metal chemistry: A self-consistent Hubbard *U* approach. *Phys. Rev. Lett.* **97**, 103001 (2006).

66. Solovyev, I. V. & Imada, M. Screening of Coulomb interactions in transition metals. *Phys. Rev. B* **71**, 045103 (2005).

67. Hu, S.-J., Yan, S. S., Zhao, M. W. & Mei, L. M. First-principles LDA+*U* calculations of the Co-doped ZnO magnetic semiconductor. *Phys. Rev. B* **73**, 245205 (2006).

68. Lee, W.-J. & Kim, Y.-S. Linear-response calculation of the effective Coulomb interaction between closed-shell localized electrons: Cu, Zn, and ZnO. *J. Korean Phys. Soc.* **60**, 781–786 (2012).

69. Wang, X. L., Tsuchiya, T. & Hase, A. Computational support for a pyrolitic lower mantle containing ferric iron. *Nat. Geosci.* **8**, 556–559 (2015).

70. Steinberg, S. & Dronskowski, R. The Crystal Orbital Hamilton Population (COHP) method as a tool to visualize and analyze chemical bonding in intermetallic compounds. *Crystals* **8**, 225 (2018).

71. Dronskowski, R. & Bloechl, P. E. Crystal Orbital Hamilton Populations (COHP): Energy-resolved visualization of chemical bonding in solids based on density-functional calculations. *J. Phys. Chem.* **97**, 8617–8624 (1993).

72. Curtarolo, S. et al. The high-throughput highway to computational materials design. *Nat. mater.* **12**, 191–201 (2013).

73. Sato, T. O. & Kaneko, H. The equilibrium diagram of the cadmium-silver-copper system. *J. Jpn. I. Met.* **6**, 75–84 (1942).

74. Kripyakevich, P., Gladyshevskii, E. & Cherkashin, E. The crystal structure of the Cu_2Cd phase. *Dokl. Akad. Nauk SSSR* **82**, 253–256 (1952).

75. Pratt, J. N. & Bryant, A. W. Thermodynamics of alloys. Calorimetric studies of maganese-copper and palladiumaluminumalloys. (University of Birmingham Department Physical Metallurgy & Science of Materials, 1969). https://apps.dtic.mil/sti/citations/AD0705644.

76. Turchanin, M. A., Agraval, P. G. & Abdulov, A. R. Phase equilibria and thermodynamics of binary copper systems with 3*d*-metals. IV. Copper-manganese system. *Powder Metall. Met. Ceram.+* **45**, 569–581 (2006).

77. Chakrabarti, D., Laughlin, D., Chen, S. & Chang, Y. Binary alloy phase diagrams, 2nd ed. *Materials Park*, 1442 (1990).

78. Nepal, N. K., Adhikari, S., Bates, J. E. & Ruzsinszky, A. Treating different bonding situations: Revisiting Au-Cu alloys using the random phase approximation. *Phys. Rev. B* **100**, 045135 (2019).

79. Hosseini, S. M., Movlarooy, T. & Kompany, A. First-principle calculations of the cohesive energy and the electronic properties of $PbTiO_3$. *Phys. B* **391**, 316–321 (2007).

80. Schimka, L., Gaudoin, R., Klimeš, J., Marsman, M. & Kresse, G. Lattice constants and cohesive energies of alkali, alkaline-earth, and transition metals: Random phase approximation and density functional theory results. *Phys. Rev. B* **87**, 214102 (2013).

81. Wu, Q., He, B., Song, T., Gao, J. & Shi, S. Cluster expansion method and its application in computational materials science. *Comp. Mater. Sci.* **125**, 243–254 (2016).

82. Richter, B., Kuhlenbeck, H., Freund, H.-J. & Bagus, P. S. Cluster core-level binding-energy shifts: the role of lattice strain. *Phys. Rev. Lett.* **93**, 026805 (2004).

83. Sham, T. K., Yiu, Y. M., Kuhn, M. & Tan, K. H. Electronic structure of ordered and disordered Cu_3Au: The behavior of the Au 5d bands. *Phys. Rev. B* **41**, 11881–11886 (1990).

84. Lu, Z. W., Wei, S.-H. & Zunger, A. Electronic structure of random $Ag_{0.5}Pd_{0.5}$ and $Ag_{0.5}Au_{0.5}$ alloys. *Phys. Rev. B* **44**, 10470–10484 (1991).

85. Kresse, G. & Joubert, D. From ultrasoft pseudopotentials to the projector augmented-wave method. *Phys. Rev. B* **59**, 1758–1775 (1999).

86. Kresse, G. & Furthmüller, J. Efficient iterative schemes for ab initio total-energy calculations using a plane-wave basis set. *Phys. Rev. B* **54**, 11169–11186 (1996).

87. Hafner, J. Ab-initio simulations of materials using VASP: Density-functional theory and beyond. *J. Comput. Chem.* **29**, 2044–2078 (2008).

88. Perdew, J. P., Burke, K. & Ernzerhof, M. Generalized gradient approximation made simple. *Phys. Rev. Lett.* **77**, 3865–3868 (1996).

89. Dudarev, S. L., Botton, G. A., Savrasov, S. Y., Humphreys, C. J. & Sutton, A. P. Electron-energy-loss spectra and the structural stability of nickel oxide: An LSDA+U study. *Phys. Rev. B* **57**, 1505–1509 (1998).

90. Baerends, E. J., Gritsenko, O. V. & Van Meer, R. The Kohn-Sham gap, the fundamental gap and the optical gap: the physical meaning of occupied and virtual Kohn-Sham orbital energies. *Phys. Chem. Chem. Phys.* **15**, 16408–16425 (2013).

91. Katriel, J. & Davidson, E. R. Asymptotic behavior of atomic and molecular wave functions. *Proc. Natl Acad. Sci. Usa.* **77**, 4403–4406 (1980).

92. Perdew, J. P., Parr, R. G., Levy, M. & Balduz, J. L. Jr Density-functional theory for fractional particle number: Derivative discontinuities of the energy. *Phys. Rev. Lett.* **49**, 1691–1694 (1982).

93. Levy, M., Perdew, J. P. & Sahni, V. Exact differential equation for the density and ionization energy of a many-particle system. *Phys. Rev. A* **30**, 2745–2748 (1984).

94. Perdew, J. P. & Levy, M. Comment on "Significance of the highest occupied Kohn-Sham eigenvalue". *Phys. Rev. B* **56**, 16021–16028 (1997).

95. Painter, G. S. Improved correlation corrections to the local-spin-density approximation. *Phys. Rev. B* **24**, 4264–4270 (1981).

96. Van de Walle, A., Asta, M. & Ceder, G. The alloy theoretic automated toolkit: A user guide. *Calphad* **26**, 539–553 (2002).

Author contributions
X.W. conceived the study. J.Z. and W.X. performed the calculations. The manuscript was written by X.W. and J.Z. All authors discussed the results and comment on the manuscript.

Competing interests
The authors declare no competing interests.

Additional information
Supplementary information The online version contains supplementary material available at https://doi.org/10.1038/s41524-024-01257-y.

Correspondence and requests for materials should be addressed to Xianlong Wang.

Reprints and permissions information is available at http://www.nature.com/reprints

Publisher's note Springer Nature remains neutral with regard to jurisdictional claims in published maps and institutional affiliations.